Off-angle to Frontal Iris Image Transformation using Pix2Pix

Generative Adversarial Networks

Jitendra S. Kota and Mahmut Karakaya

5 Kennesaw State University, College of Computing and Software Engineering, Marietta, USA, 30060

Abstract Iris recognition is a reliable biometric identification method known for its low false acceptance rates. However, capturing ideal iris images is often challenging and time-consuming, which can degrade the performance of iris recognition systems when using non-ideal images. Enhancing iris recognition performance for non-ideal images would expedite and make the process more flexible. Off-angle iris images are a common type of non-ideal iris images and converting them to their frontal version is not as simple as making geometric transformations on the off-angle iris images. Due to challenging factors such as corneal refraction and limbus occlusion, the frontal projection requires a more comprehensive approach. Pix2Pix GANs, with their pairwise image conversion capability, provide the ideal foil for such a tailored approach. This paper demonstrates how Pix2Pix GANs can effectively be used for the problem of converting off-angle iris images to frontal iris images. This paper provides a comprehensive exploration of techniques using Pix2Pix GAN to enhance off-angle to frontal iris image transformation by introducing variations in the loss functions of Pix2Pix GAN for better capturing the iris textures and the low contrast, changing the medium of input from normalized iris to iris codes, and ultimately delving deeper into studying which regions of the Gabor filters contribute the most to iris recognition performance.

- **Keywords**: biometrics, iris recognition, off-angle iris, iris feature extraction, generative images, GAN.
- 20 E-mail: <u>mkarakay@kennesaw.edu</u>

1 Introduction

Iris recognition has quickly emerged as one of the most promising biometric identification approaches, given its low false acceptance rates and the contact-less nature of the process. Iris recognition utilizes distinctive characteristics found in the iris of a person's eye to differentiate one individual from another. Most existing iris recognition systems use frontal iris images, captured when a person is directly looking at the camera. However, capturing frontal iris images is not always possible. If a person looks in a different direction when the images are captured, the quality of iris images captured is not deemed good and might warrant a recapture of the image and can lead to time wastage. This signifies the importance of constructing an unconstrained iris

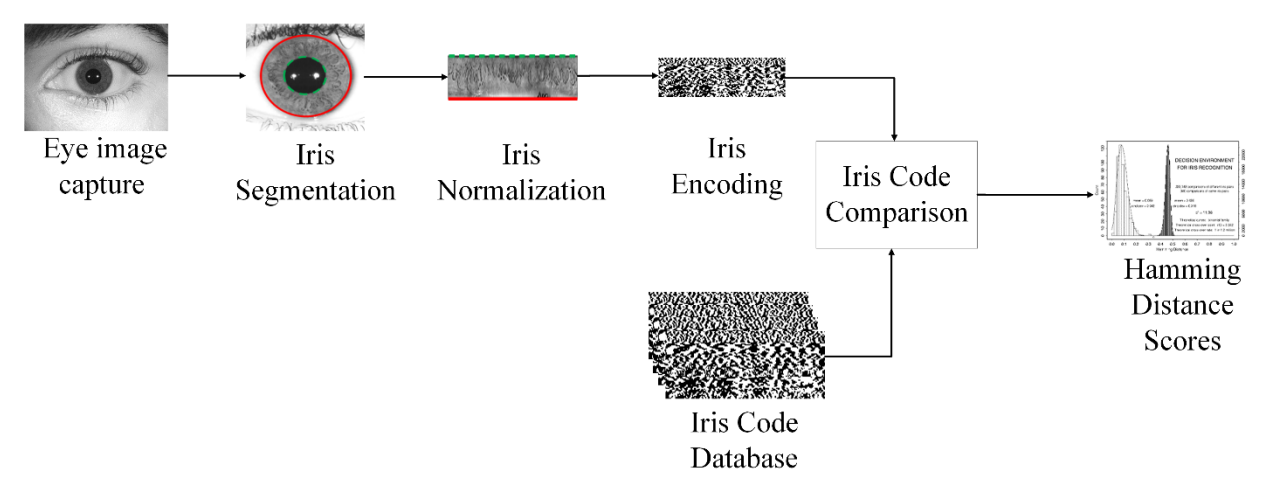


Fig. 1. General process of iris recognition.

recognition model capable of performing off-angle iris recognition. Additionally, frontal

31

32

33

34

35

36

37

38

39

40

41

42

43

44

45

restriction limits iris recognition to merely using it as a stationary biometric identification. Offangle iris recognition models can help create dynamic biometric identification systems that can be used to accelerate person identification on the go and assist in capturing suspected criminals on the run. Some of the challenges faced in frontal iris recognition systems are iris occlusion due to eyelids and blurred images. In addition to these, off-angle iris recognition systems face a few more challenges, namely, corneal refraction, limbus occlusion, and the 3-Dimensional structure of the iris. Firstly, there is the distortion caused due to the presence of cornea. Since cornea contains water, majorly, the light refracts due to the difference in refractive indices of air and water. However, this refraction occurs differently for different gaze angles making this an issue. Then there is the three-dimensional nature of iris, which can create shadows on the iris plane. Also, a depth of field blur is caused because the iris plane is not parallel to the image plane in off-angle scenarios. In addition to these, there is the presence of limbus, which is a semi-transparent tissue, whose presence can be magnified at extreme angles, thereby occluding some pixels leading to loss

of useful information. These challenges mean that simple geometric transformations are not sufficient to convert an off-angle iris image into its frontal version.

46

47

48

49

50

51

52

53

54

55

56

57

58

59

60

61

62

63

64

65

66

67

In general, as seen in Fig. 1, iris recognition involves capturing eye images using near-infrared cameras to be able to better capture the low-contrast iris patterns. Second, the inner and outer iris boundaries are segmented. Third, the iris portion of the eye is unwrapped into a rectangular strip by sampling from the original annular structure by using Daugman's Rubber Sheet model.² This rectangular strip is called the normalized iris image. Fourth, the normalized iris image is convolved with three different Gabor filters, resulting in six different binary strips. The combined binary image is called as iris code. Finally, the iris code is compared with all the iris codes stored in the database calculating Hamming distance scores. The Hamming distance scores for iris images belonging to the same eye, also referred to as intra-class hamming distance scores, would be lower compared to the hamming distance scores for the irises coming from different eyes, also referred to as inter-class hamming distance scores. During the hamming distance calculation, eyelid masks are applied to ensure that the comparison is only done on iris pixels and not on other eye structures. When off-angle iris images are used during inference in the above process directly, without any further processing, the gap between the intra-class Hamming distance scores and the inter-class Hamming scores becomes smaller, leading to greater misclassifications. This highlights the need to consider off-angle iris recognition as a standalone problem. This paper takes the approach of attempting to project off-angle iris images into their frontal views to improve the performance of off-angle iris recognition. To accomplish this, the paper utilizes the Pix2Pix GAN model and adapts it to the context of iris images. This paper adopts three different approaches that have been considered for the frontal transformation process. The paper is structured as follows: section 2

offers background information, section 3 describes the three different conversion approaches and the loss functions, section 4 presents the results and discussion, and section 5 concludes and showcases potential future work.

2 Related Work

68

69

70

71

72

73

74

75

76

77

78

79

80

81

82

83

84

85

86

87

88

89

The initial implementation of iris recognition was expected to capture frontal iris images.² It used the Gabor-phase quadrant feature descriptor to convert normalized iris images into binary iris codes. These iris codes were compared with codes in a previously recorded database for identification by calculating Hamming distances. In addition to the iris codes, several other feature descriptors such as Scale-Invariant Feature Transform (SIFT) features³ were also proposed. Frontal iris feature extraction was explored using deep learning mechanisms such as ResNet-50.4 and spatial attention.⁵ Frontal iris recognition algorithms faced challenges when compared with off-angle iris images. One of the main challenges was the effect of gaze angle. To counter this, several approaches were proposed including affine transformations to project off-angle images into frontal, ⁶ ellipse fitting to off-angle images for segmentation and normalization, and Support Vector Machines to extract features.⁸ However, these approaches did not improve the recognition for off-angle images captured at gaze angles exceeding 30° because they assumed a flat iris and ignored light refraction at the cornea, which was another major challenge for off-angle iris recognition. Santos-Villalobos et al.⁹ employed the ray-tracing method to compute the impact of corneal refraction on off-angle iris images and proposed a conversion technique to generate frontal versions. This method proved successful for synthetic images but failed with real images due to the presence of the limbus, which presented an additional challenge affecting off-angle iris recognition. Karakaya et al. 10,11

investigated the effects of limbus occlusion and the three-dimensional structure of the iris on offangle iris recognition. They observed that the presence of the limbus increased the intra-class Hamming distance scores, bringing them closer to inter-class scores, particularly at higher gaze angles.

Convolutional Neural Networks (CNN) have been used for improving off-angle iris recognition performance as well. A Transfer Learning based approach on the iris, ocular, and periocular modalities¹² using different training set combinations of gaze angles, revealed that using off-angle iris images in training makes testing more robust as opposed to using frontal images alone. Another approach involved using Triplet loss functions¹³ in CNNs to extract features. This approach showed good performance at gaze angles greater than 30°, but the CNN seemed to utilize non-iris regions for recognition more than the actual iris portions.

The advent of generative models has given rise to multiple context-based generative models. While image generation based on seed images has been explored in various domains, such as face images, extending these techniques to iris images is challenging. Zhang et al. ¹⁴ used a Conditional Adversarial Autoencoder for generating face images corresponding to different ages, but this approach does not apply to iris images, as the traversal in latent space does not guarantee a traversal across different gaze angles. GANs, on the other hand, have proven effective for generating realistic images. Conditional Generative Adversarial Networks (CGANs) use label information to generate images of specific classes. Taherkhani et al. ¹⁵ employed CGANs to match profile face images with their frontal versions, using a U-Net architecture for generators and a patch-based discriminator. They proposed using generative modeling to project profile and frontal face images into a latent space for face matching and frontal face generation. On a similar note, the Pix2Pix

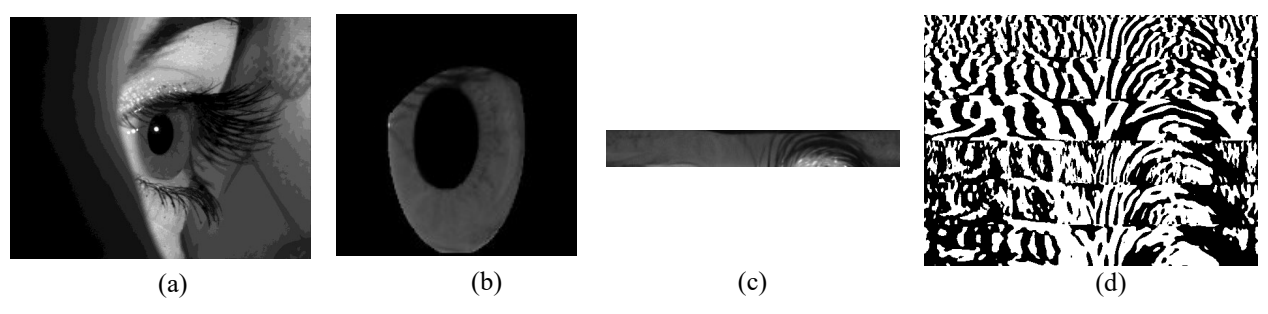


Fig. 2. Different domains for iris image conversion (a) Captured original image (b) Ocular iris image (c) Normalized iris image (d) Iris code with six-channels.

GAN model¹⁶ demonstrated how an image in one domain space can be converted into an image in another domain space. In the current paper, we propose an open-set solution to the iris recognition problem by employing a modified Pix2Pix architecture which can be used to convert off-angle iris images to frontal iris images.

3 Methodology

To use the Daugman's² pipeline for traditional iris recognition, the possible domains for image conversion are the original captured eye images, the ocular iris images, the normalized iris version, and the iris code version, as can be seen in Fig. 2. The problem with using the original eye images is the presence of other structures like the eyelids, eyebrows, sclera, and the pupil. All other structures, which usually have a higher contrast and greater edge separations, are bound to dominate the conversion process, without attributing enough emphasis to the iris portion of the image. The ocular iris images also face a similar problem due to the presence of sclera, and the pupil portions. The normalized iris image and the iris codes are the best options for iris image conversion, as these images only concentrate on the iris portion. One problem with using images in these domains is that the output can only be a normalized or an iris code image, and not an actual eye image. However, this information is sufficient for iris recognition.

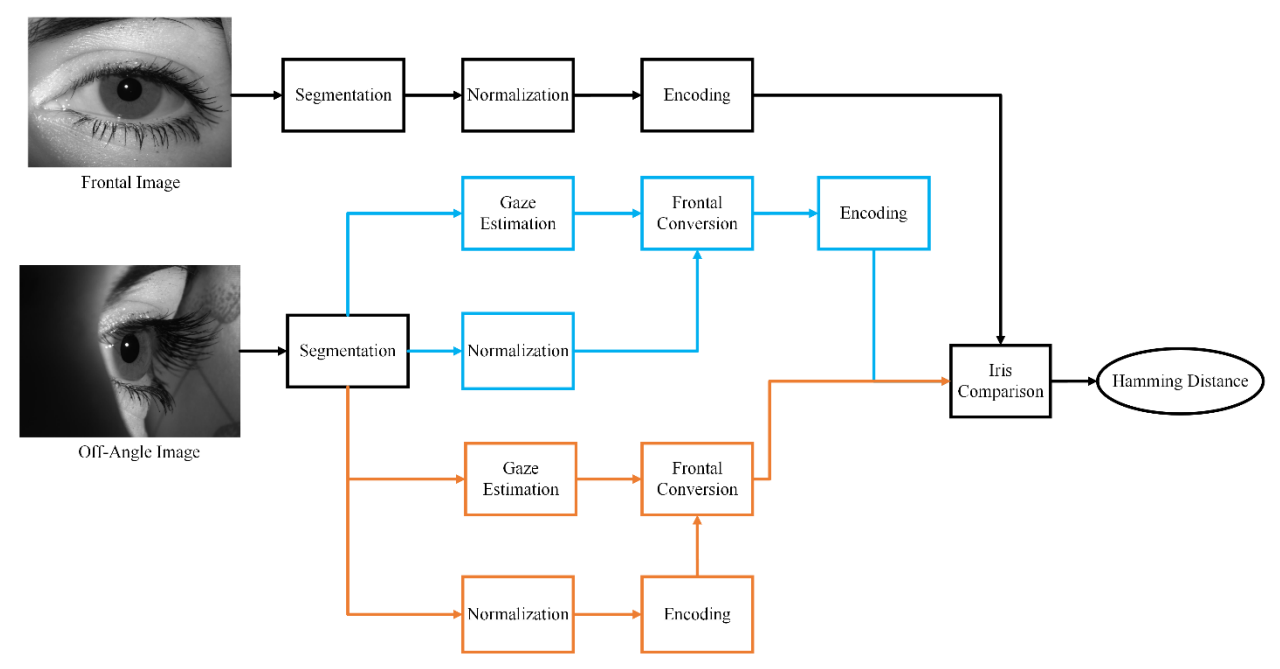


Fig. 3. Approaches to frontal iris conversion – using Normalized iris images (blue) and using Iris Code images (orange).

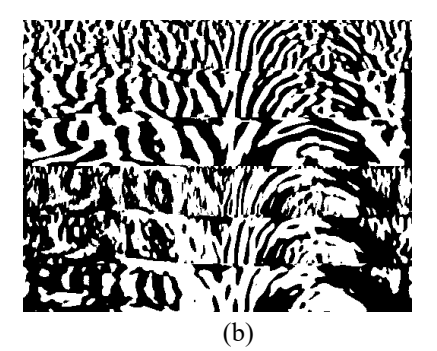
Using normalized images and the iris codes, we propose three different models for off-angle to frontal iris image projection. The first one uses only the normalized iris images, the second one uses the iris codes, and the third one uses sub-blocks of iris codes. They are described in the following subsections.

3.1 Conversion using Resized Normalized Iris Images

This approach¹⁷ utilizes two separate branches. As can be seen in Fig. 3, the first branch employs the traditional method suggested by Daugman² on the frontal iris images for generating a normalized frontal iris image dataset. This branch follows the steps of image capturing, segmentation, normalization, and then encoding into iris codes. The normalized iris images, originally sized 64x512, were resized to 256x256 using bilinear interpolation to ensure smooth scaling and to also achieve the dimensions suitable for the Pix2Pix GAN network. Consequently,

139 the eventual frontal iris code dataset would also comprise (256 x 256) images. This dataset will 140 then be used later for comparison with the probe images. 141 The second branch, highlighted with blue color in Fig. 3, in this process attempts to generate a new 142 iris image by converting off-angle normalized iris images to their frontal version. After iris capturing and iris segmentation,² the gaze angle of the off-angle iris image is calculated using a 143 gaze estimation method.¹⁸ Simultaneously, the segmented off-angle iris image is normalized.¹⁹ 144 Both the gaze angle and the off-angle normalized iris image are sent as inputs to an Off-angle to 145 146 Frontal iris converter. This converter resizes the (64 x 512) off-angle normalized iris images to 147 (256 x 256) off-angle normalized iris images and outputs a (256 x 256) generated frontal iris image. 148 This generated frontal iris image is encoded to create a (256 x 256) generated iris code. This 149 generated iris code acts as the probe image and is compared with the frontal iris code database. 150 The result of the comparison is a Hamming distance score, which is expected to be low for intra-151 class cases and high for inter-class cases. 152 The off-angle to frontal iris converter employs a Pix2Pix GAN model with additional Generator loss functions. The generator of this model is a U-net model, ¹⁶ featuring an encoder and a decoder, 153 154 with skip connections. There are 8 down-sampling instances in the encoder before reaching the 155 bottleneck, followed by 7 up-sampling instances in the decoder. Each down-sampler has a 156 Convolution, Batch Normalization, and a ReLU layer. Similarly, each up-sampler has a 157 Transposed Convolution, Batch Normalization, and a Dropout layer. The discriminator is a patchbased discriminator, ¹⁶ which works at a patch level instead of an image level. 158





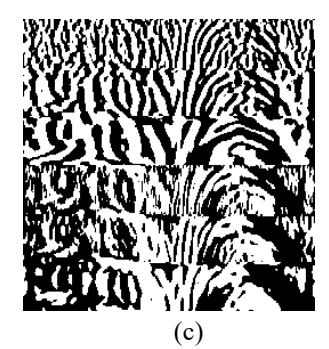


Fig. 4. Sample images (a) Off-angle image, (b) Original iris code (384 x 512), (c) Resized iris code (256 x 256).

3.2 Conversion using Resized Iris Code Images

This approach is identical to the Resized Normalized Iris approach, except that the iris codes are used directly for iris conversion instead of the normalized iris images. As shown in Fig. 3, the first branch of the model is the same as the first branch in the normalized approach. In the second branch, highlighted with orange color in Fig. 3, an additional step of converting the off-angle normalized iris images to iris code is performed before sending the images to the Iris Converter. The iris code images are resized to (256 x 256), in a similar fashion to the normalized approach. One possible advantage of resizing at the iris code level instead of the normalized iris level is that the iris code images, which originally have a shape of 384 x 512 are closer to the resized shape of (256 x 256) than the normalized images, which originally have a shape of (64 x 512). This could mean that there would be fewer stretched and contracted areas in this case.

3.3 Conversion using Iris Code sub-blocks

The iris codes generated by the Gabor filters consist of six different strips. The first three strips are referred to as real parts, while the last three strips are referred to as imaginary parts. Therefore, the resultant iris code image has a size of (384 x 512). In approach 3.2, we resized this iris code to a (256 x 256) iris code image. However, this resizing process could lead to stretching and contracting

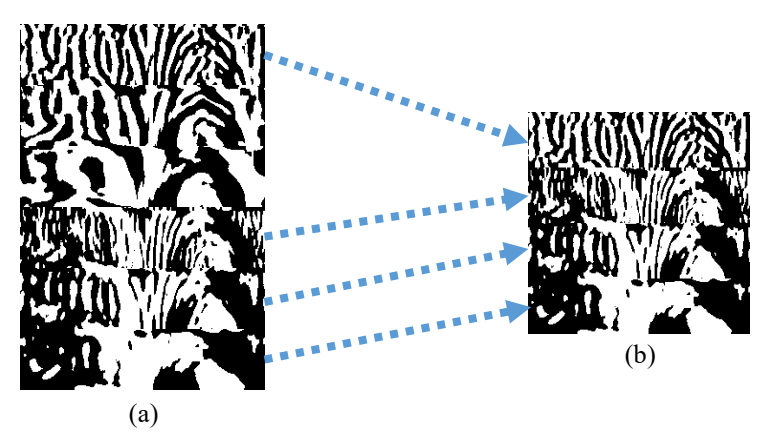


Fig. 5. Choosing sub-blocks of iris code: (a) Original iris code with six channels (384 X 256) (b) Iris code sub-block with four channels (256 X 256).

of certain iris code portions, resulting in inconsistencies along the edges of patterns inside the iris code and potential performance deterioration, as seen in Fig. 4.

In the iris code sub-blocks approach, the primary objective is to prevent such stretching or contractions. Instead of sampling the normalized image as (64×512) , the sampling is performed in a way that yields (64×256) normalized images. Gabor filters are then applied to these normalized images, resulting in $6 * (64 \times 256)$ iris code images. From these six different iris code strips, four strips are selected combinatorically, resulting in $4 * (64 \times 256)$ iris code images, as can be seen in Fig. 5. Since this is an exhaustive search, a total of $\binom{6}{4}$ combinations are explored to avoid a potential bias and provide us insights into the portions of the iris image that are the most informative and beneficial for the iris recognition task.

This approach ensures the extraction of a (256 x 256) iris code image without any stretching or contractions. Similar strips are created for both off-angle and frontal iris code images. These (256 x 256) iris code images are handled in the same manner as in approach 3.2.

3.4 Loss functions

Iris images have low contrast and complicated textures, which are important to be identified in the iris recognition process. So, it is important to identify loss functions that can capture these two qualities of iris images. So, we have added two more loss functions to the generator to incorporate these qualities. In addition to the two loss functions used by the original Pix2Pix GAN in (i) Binary Cross Entropy loss function (L_{CGAN}), and (ii) L1 loss (L_{L1}), we use a combination of Structural Similarity Index (SSIM) and Matrix Multiplication loss functions.

On one hand, the Binary Cross Entropy loss function forces the generator to make realistic images, and on the other hand, the loss function forces the discriminator to better distinguish the real images from the images generated by the generator. L1 loss is used only on the generator side to minimize the gap between the generated and the original images, by reducing the mean absolute difference between the pixels of the two images.

200 These two loss functions can be expressed as follows:

$$L_{CGAN} = E_y[log D(y)] + E_{x,z} \left[log \left((1) - D(x, G(x, z)) \right) \right]$$
(1)

$$202 L_{L1} = E_{x,y,z}[||y - G(x,z)||] (2)$$

where D is the discriminator, G is the generator, x is the input off-angle normalized iris image, y is the original real frontal normalized iris image, and z is random noise.

The first of the two new loss functions introduced in this modified version of Pix2PixGAN is the Matrix Multiplication loss function. This loss function is calculated using the mean dot product of the generated and the original image pixel values. The pixel-wise interactions between the generated and the original images would penalize textural and structural changes between the

- original and the generated image, thereby ensuring that the generated images are as close to the original images as possible.
- The Matrix Multiplication loss can be expressed as:

$$L_{MM} = E_{x,y,z}[y * G(x,z)]$$
 (3)

- 213 where G is the generator, x is the input off-angle iris image, y is the original real frontal normalized
- 214 iris image, z is random noise, and L_{MM} is the Matrix multiplication loss function.
- 215 Structural Similarity Index (SSIM) loss function²⁰ is the second loss function that we have added.
- 216 SSIM loss function captures three aspects of the image such as luminance, contrast, and structure.
- 217 Luminance captures the overall intensity of the image. Contrast identifies the changes in intensities
- amongst the different regions of the image. The unique spatial arrangement of different features in
- the iris image can be identified using Structure. The expressions for luminance, contrast, and
- 220 structure are as follows:

$$\mu_{x} = \frac{1}{N} \sum_{i=1}^{N} x_{i} \tag{4}$$

222
$$\sigma_{x} = \left(\frac{1}{N-1} \sum_{i=1}^{N} (x_{i} - \mu_{x})^{2}\right)^{\frac{1}{2}}$$
 (5)

$$s_{x} = \frac{(x - \mu_{x})}{\sigma_{x}} \tag{6}$$

- where μ_x (luminance) is the mean value of all pixels, σ_x (contrast) is the standard deviation, and
- 225 s_x (structure) is the normalized version of intensity.

The formulae for the comparison of luminance, contrast, and structure for two different images are as follows:

$$l(x,y) = \frac{2\mu_x \mu_y + C_1}{\mu_x^2 + \mu_y^2 + C_1}$$
 (7)

$$c(x,y) = \frac{2\mu_x \mu_y + C_2}{\mu_x^2 + \mu_y^2 + C_2}$$
 (8)

$$s(x,y) = \frac{\sigma_{xy} + C_3}{\sigma_x \sigma_y + C_3} \tag{9}$$

- where l(x, y), c(x, y), and s(x, y) are the comparative measures for luminance, contrast, and
- structure for the off-angle input iris image x and the expected real frontal iris image y. C_1 , C_2 , C_3
- are the constants.

242

234 The final expression for SSIM is given as follows:

235
$$SSIM(x,y) = [l(x,y)]^{\alpha}.[c(x,y)]^{\beta}.[s(x,y)]^{\gamma}$$
 (10)

236
$$L_{SSIM} = \frac{(2\mu_x \mu_y + C_1)(2\sigma_{xy} + C_2)}{(\mu_x^2 + \mu_y^2 + C_1)(\sigma_x^2 + \sigma_y^2 + C_2)}$$
 (11)

- where L_{SSIM} is the SSIM loss function.
- Using (1), (2), (3), and (11), the final generator loss function for the conversion of off-angle iris
- 239 images to their frontal versions is given as follows:

$$L_{total} = L_{CGAN} + \lambda L_{L1} + L_{MM} + L_{SSIM}$$
 (12)

where λ is the regularization parameter and is set at 100, which yielded images with higher visual

quality. The authors in the original Pix2Pix GAN paper have also stated that 100 as a regularization

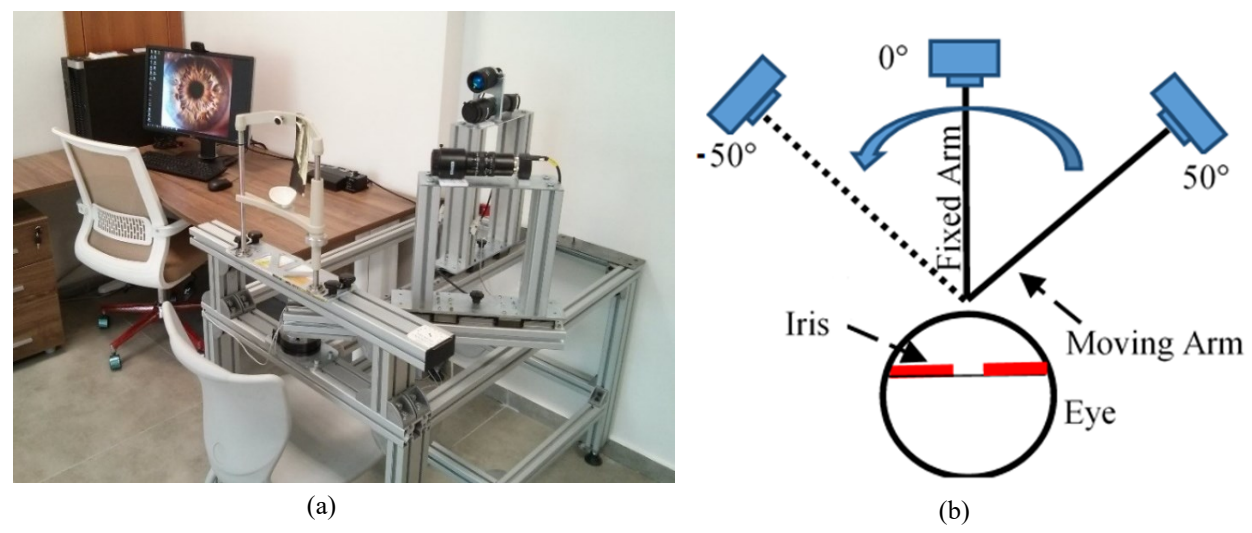


Fig. 6. (a) Experimental setup of off-angle image capturing (b) Illustration of the movement of the camera.

parameter provides a good balance between reconstruction fidelity and avoid overfitting, resulting in minimal blurring and visual artifacts.¹⁶

4 Experiments and Results

For our experiments, two IDS-UI-3240ML-NIR cameras have been used to capture off-angle and frontal iris images at the same time as shown in Fig. 6. The frontal iris images are captured using a fixed camera, in front of the subject. The off-angle iris images are captured using a moving camera, which moves horizontally from -50° to +50° around the subject. The frontal camera is 82 cm away from the eye and the off-angle camera is rotated at 48 cm away. Navigator Zoom 7000 lenses have been used for both cameras, with the focal length of the stationary camera set at 108 mm, while that of the moving camera is set at 40 mm. A 780 nm M780L3-C1 Collimated high-power LED light source is used as the illuminator, and a 720 nm high-pass infrared filter is used to improve the image quality. Navigator Zoom 7000 lens is a manual lens that can be fixed to the focal length at 18-108mm range. Moving camera makes horizontal movement from 50° in angle to -50° in angle. The base of the moving camera is mounted on a rotary table controlled by a step

motor. Before starting the data capture, the off-angle camera is moved to +50° in angle position and frontal camera is always at 0° in angle position. After the subject put his head into the chin rest, the chin rest is moved into left-right and front-back to make sure the left eye is at the center of the rotation. Therefore, both cameras are focused on the eye and their depth of focus is sufficient to maintain well focused images while moving the off-angle camera from 50° in angle to -50° in angle. The captured images are shown on a monitor to ensure image sharpness during the data capture. The iris images from the left eye are captured first and the process is repeated for the right eye. The moving camera captures 10 images at 10° increments, which would account for a total of 110 off-angle iris images for the 11 different angles ranging from -50° to +50°. The head is stabilized using a chin rest, to ensure that the axes of the subject and the eye align. The dataset consists of 24360 iris images from 100 subjects, out of which 64 are male and the rest are female where the average age is 26. In our experiment, we only included the iris images from the left eye captured at gaze angles greater than 30 degrees from the moving camera to study the effects of frontal projection at extreme angles. This accounted for 6391 images, with 913 images for each of +30°, +40°, +50°, 0°, -30°, -40°, and -50° gaze angles. We created five different cross-folds on the subject level using a split of 80%-20% train-test split on the dataset. Therefore, we guarantee that training and testing images come from different subjects, and every image in the dataset is tested once. We present the results for only left eye due to the availability of the ground-truth segmentation. The models were evaluated on a MacBook Air equipped with 8GB of RAM, and an Apple M1 chip processor. The average processing time for converting an off-angle image to its frontal counterpart was recorded at 0.0945 seconds.

257

258

259

260

261

262

263

264

265

266

267

268

269

270

271

272

273

274

275

276

277

278

Hamming distance scores are used for comparison between the iris codes as a performance metric. For iris images belonging to the same subject, the hamming distance scores are expected to be lower than the hamming distance scores of iris images belonging to two different subjects. We have set the baseline as the hamming distance scores between original off-angle and frontal iris images. Each conversion approach generates different sets of converted frontal iris images, whose hamming distance scores are then compared with the baseline model. The corresponding Receiver Operating Curves (ROC) and the Area Under Curves (AUC) are compared as well to determine the efficiency of the approach. The formula for Hamming distances is as follows:

287
$$HD = \frac{||(c_A \oplus c_B) \cap (m_A \cap m_B)||}{||m_A \cap m_B||}$$
 (13)

ROC curves were drawn with a minimum threshold of 0.35 and a maximum threshold of 0.6. We arrived at these values after evaluating the range of Hamming Distance scores obtained for both the off-angle iris images. An increment of 0.00001 was used at each point in the ROC curve to toggle the threshold value. This is used to evaluate the number of true positives and false positives. Any Hamming Distance comparison value falling below the threshold at each point for the same subject is considered as a True Positive and any point falling below the threshold for different subjects is considered as False Positive. Similarly, any point falling above the threshold for different subjects is considered as True Negative, and any point falling above the threshold for different subjects is considered as True Negative. True Positive Rate (TPR) and False Positive Rate (FPR) are computed using the following formulae:

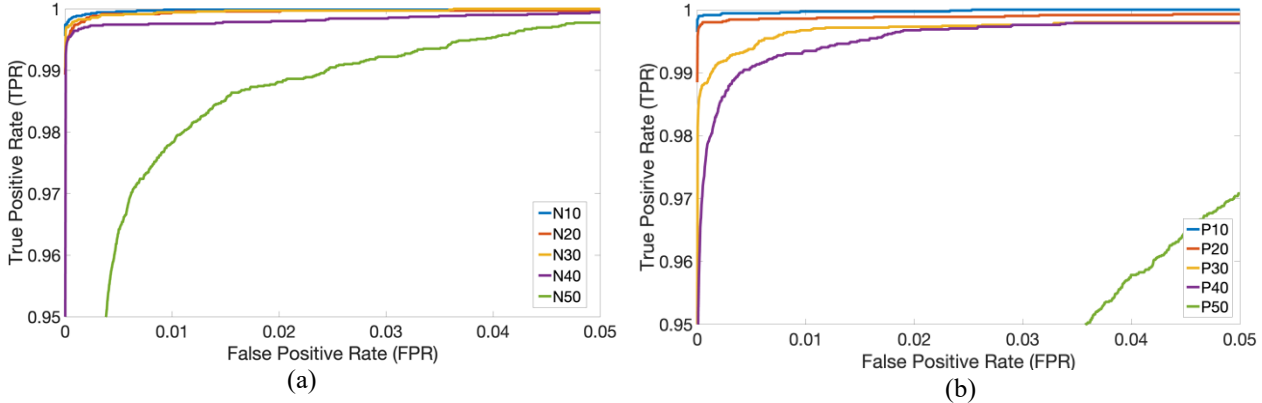


Fig. 7. Baseline ROC curves for all the subjects in (a) Negative gaze angles (b) Positive gaze angles.

ROC is then constructed by changing the Hamming Distance threshold values and calculating the corresponding TPR and FPR. The AUC values are then computed using the trapezoidal rule, which is a numerical integration tool used to approximate the area under a curve. The baseline ROCs for the positive and negative gaze angles for the left iris images are presented in Fig. 7. As can be observed, the performance of both the positive and negative extreme gaze angles such as 40° and 50° deteriorate when compared to the lower angles. Another thing to take notice of is the much lower performance of the positive gaze angles when compared to the negative gaze angles. This performance deterioration has to do with the difference in the visual and geometric axes of the eye. There is an 8° angle between the camera and the eye. As a result, the +50° gaze angle becomes more like a +58° gaze angle image, making this the most severe of all the gaze angles. Angle Kappa which is the difference between the pupillary and visual axis of an eye is estimated to be about 8° in angle, which does make the -40° gaze angle images closer to -32° gaze angle images and the -50° images closer to the -42° gaze angle images. This also means that the positive angles of +40° degree and +50° degree gaze become closer to +48° degree and +58° degrees.

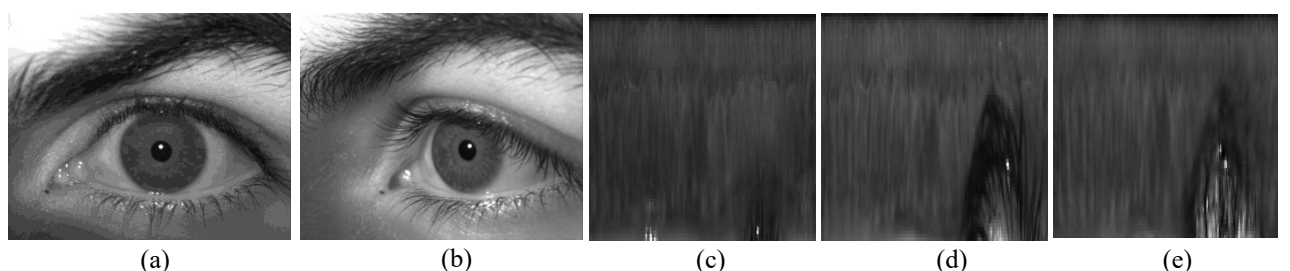


Fig. 8. A test subject's (-40° gaze angle) (a) Frontal iris image (b) Off-angle iris images (c) Resized frontal normalized iris images (d) Resized off-angle normalized iris image (e) Generated normalized iris image.

4.1 Experiments for Conversion using Resized Normalized Iris Images

314

315

316

317

318

319

320

321

322

323

324

325

326

327

328

329

The first approach utilizes resized normalized iris images for frontal iris projection. To demonstrate this approach, we use the frontal and off-angle left eye images in Fig. 8 (a, b). After segmentation of the iris region, we used elliptical unwrapping to normalize these images. The images are then resized to (256 x 256) since the Pix2Pix GAN model requires an input size of (256 x 256). The corresponding normalized images for off-angle, frontal, and generated frontal iris using the modified Pix2ix GAN are displayed in Fig. 8 (c, d, e). The darker structures in each image are the eyelids. Even to the naked eye, the texture, and the structural formations of the normalized iris images in Fig. 8 (c) and Fig. 8 (d) are much different from one another as opposed to the texture and the structural formations of the normalized iris images in Fig. 8 (c) and Fig. 8 (e). This shows the effect of using the normalized approach visually. When we compare the test subject with 19 other subjects for inter-class evaluations, we noticed in Fig. 9 (a, b) that the overlap between intra-class and inter-class hamming distance plots decreases using the proposed approach, when compared to the overlap between intra-class and inter-class hamming distance plots in the original off-angle iris images. Also, their corresponding ROC curves (see Fig. 9 (c)) indicate the improved performance of the proposed model.

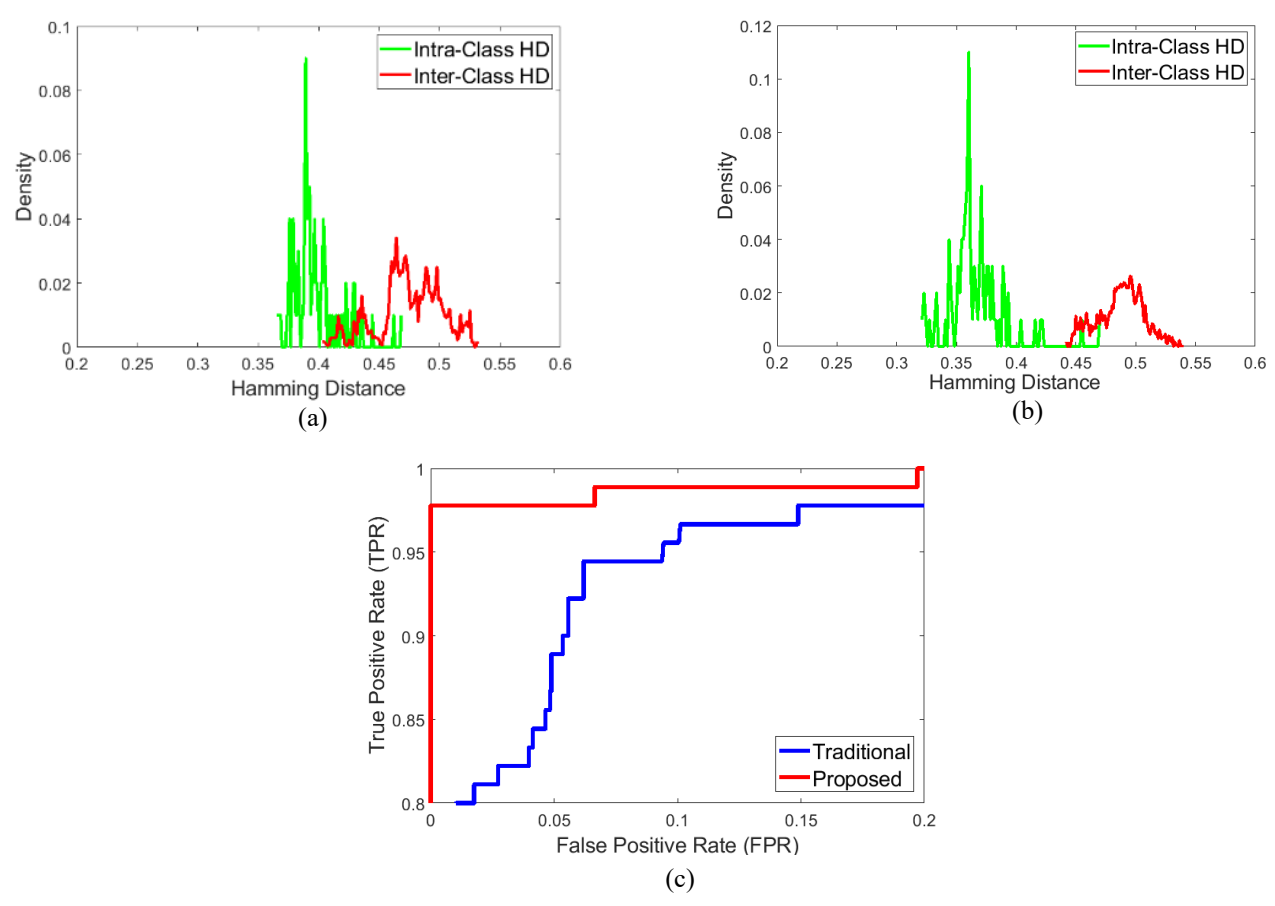


Fig. 9. Distributions of hamming distance scores for: (a) the frontal vs. off-angle iris images (-50° in angle) (b) the frontal vs. generated frontal images for the test subject (c) Performance analysis using ROC plots images at -50° in angle vs. generated frontal images for the test subjects.

To evaluate how well the proposed model with its loss functions works as opposed to models with other loss functions, several combinations of Wasserstein loss, ²¹ SSIM loss, ²⁰ L1 loss, and Matrix Multiplication loss functions are used. For this experiment, the off-angle iris images at -50° gaze angles are used, where 85% of the images are used for training, and the rest are used for testing. The first combination of loss functions included L1 loss, SSIM loss, and Wasserstein loss function applied at the pixel level. The second loss function included L1 loss, SSIM loss, and Wasserstein loss function without the mean. The third loss function only had the L1 loss. The fourth loss function included L1 loss, SSIM loss, and Matrix Multiplication loss function. Fig. 10 illustrates

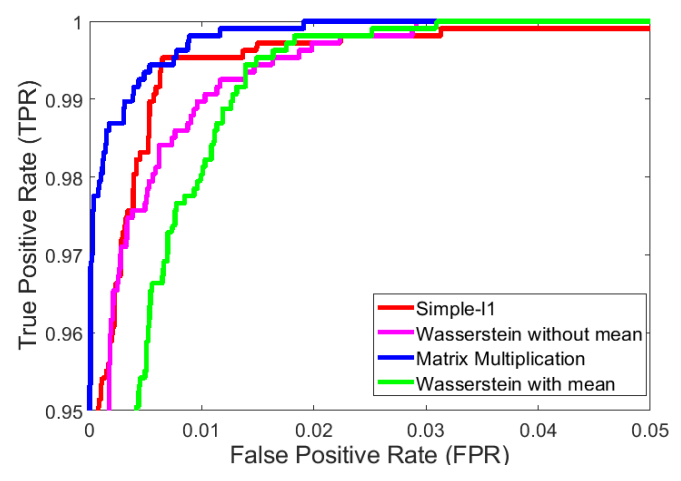


Fig. 10. Performance analysis using ROC plots for off-angle images at -50° in angle for different loss functions.

339

340

341

342

343

344

345

346

347

348

349

350

351

352

that the fourth loss function, employing the Matrix Multiplication loss, demonstrated superior performance compared to the other loss functions, suggesting it is the most effective among them. However, the improvement in iris recognition performance using the proposed approach is not consistent. As can be seen in Fig. 11, this model improved performance at only the negative angles, -40° and -50°, while not being able to manage the same at positive angles +40° and +50°. The Area Under Curve (AUC) has improved from 0.989 to 0.994 for -40° gaze angle images, while the AUC improved from 0.907 to 0.959 for -50° gaze angle images. The Equal Error Rate for -40° gaze angle images remained at 0.002, while it improved from 0.014 to 0.008 for -50° gaze angle images. The images at -30° and +30° gaze angles already had perfect ROC curves, leaving little room for improvement. This reiterates the need for more investigation of gaze angles beyond 30°. More specifically, out of the 100 subjects, for -50° gaze angle images, the performance deteriorated for two subjects due to the excessive presence of limbus, and occlusion of the iris view, because of the extremity of the angle. The performance improved for three other subjects. For -40° gaze angle images, the performance improved for two subjects which had high contrast iris structures and deteriorated for one subject with low contrast iris structure. For +40° gaze angle images, 11

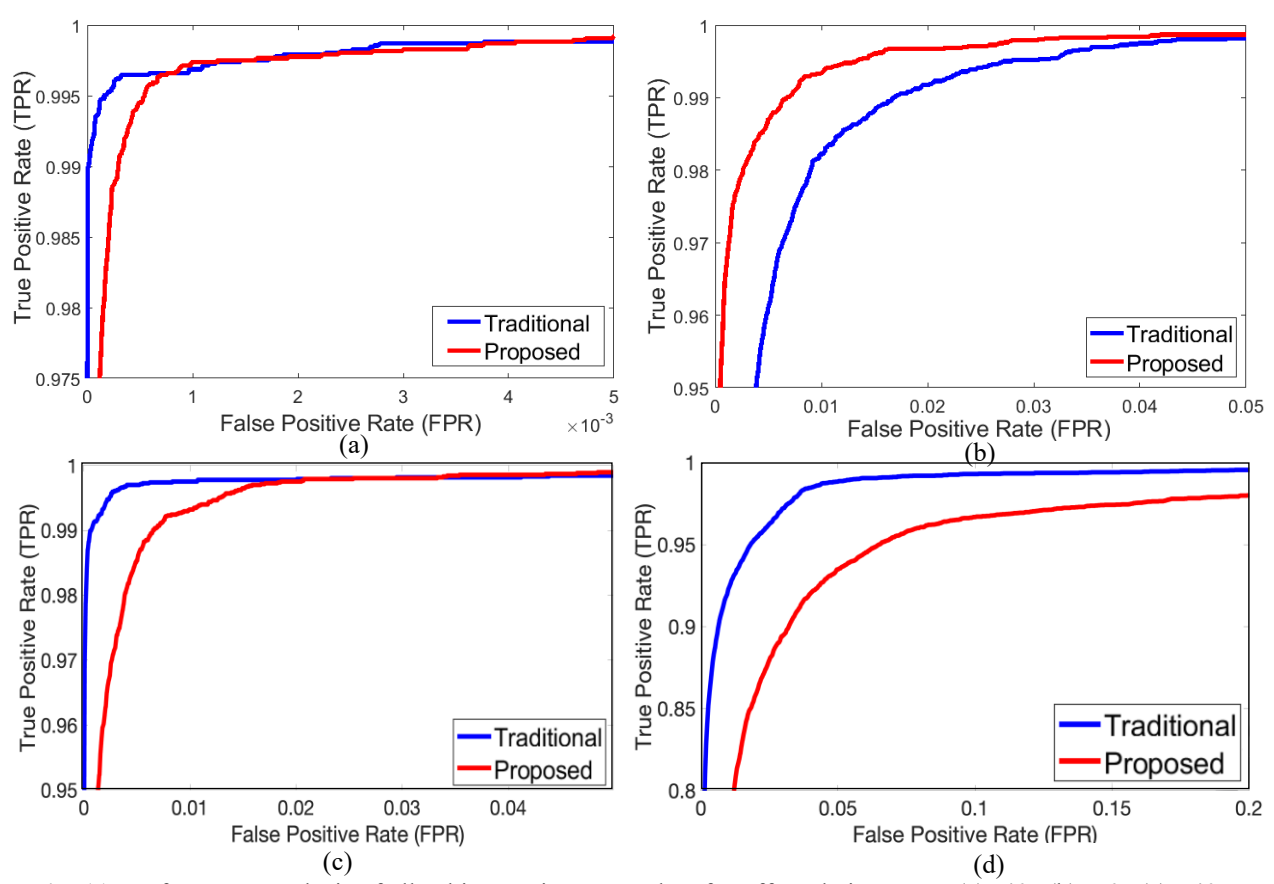


Fig. 11. Performance analysis of all subjects using ROC plots for off-angle images at (a) -40° (b) -50° (c) $+40^{\circ}$ (d) $+50^{\circ}$ in angle using resized normalized iris images.

out of the 100 subjects yielded better performance, whereas another 11 subjects showed a lower performance than the baseline. These images suffered from low contrast iris structures, 3D structure of the iris, and an uneven limbus. In addition to the corneal refraction, limbus occlusion, eyelids, and low contrast images, some subjects' noses occluded the iris images at +50° gaze angle. A total of 14 subjects has some portion of their iris occluded by their nose at +50° gaze angle. These results indicate that a more complicated approach than simply using the normalized is required in this case.

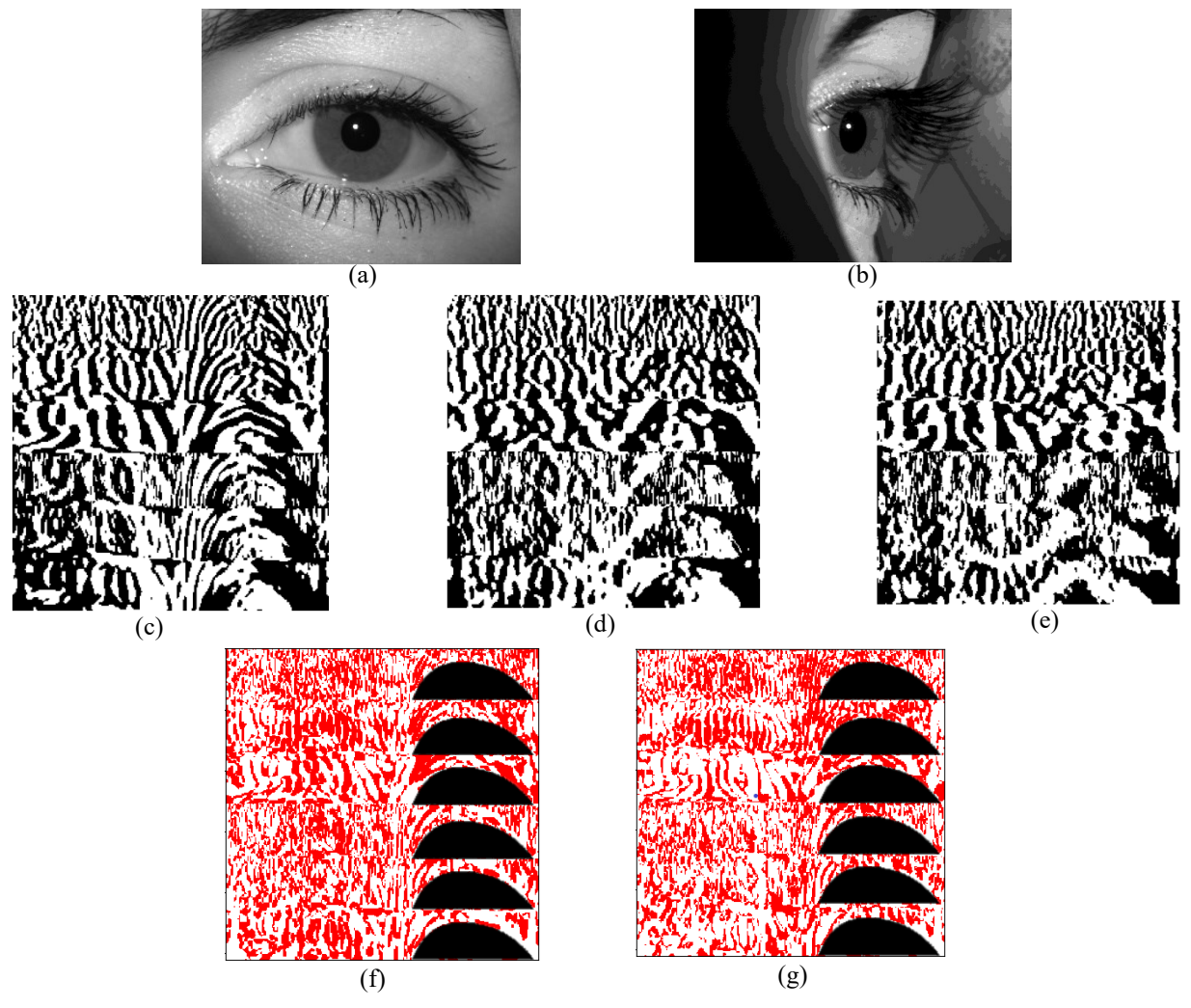
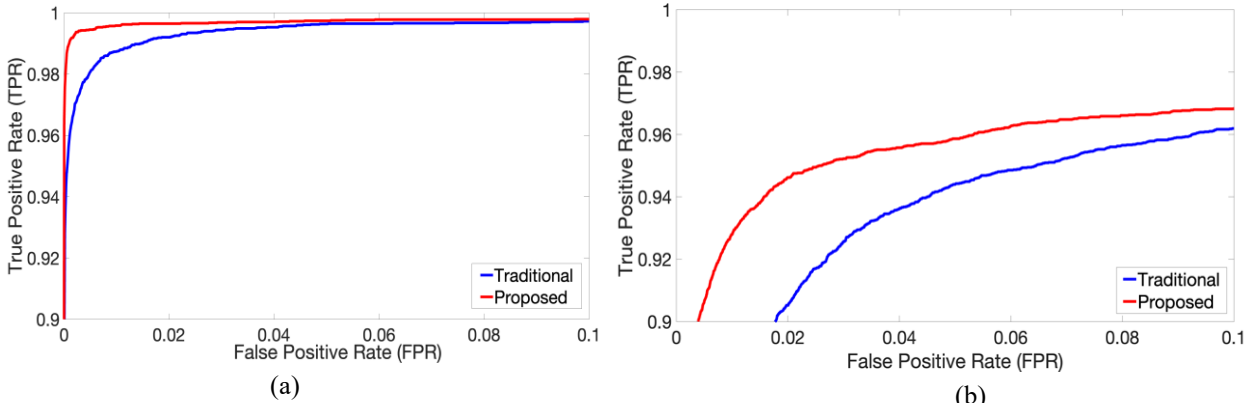


Fig. 12. A test subject's: (a) Frontal eye image (b) Off-angle iris image, Iris codes of (c) frontal, (d) off-angle, (e) generated images. XOR comparison of (f) frontal and off-angle iris codes and (g) frontal and generated iris codes. Note that, red pixels are for different bits (misses), white for same bits (hits), and gray for the mask.

4.2 Experiments for Conversion using Resized Iris Codes

The second approach for frontal iris projection utilizes the resized iris code images. In this approach, the (384 x 512) iris code images are resized into (256 x 256) to fit the Pix2Pix GAN network. To demonstrate the effect of this model, we use a test subject as shown in Fig. 12 (a, b). Here, Fig. 12 (c) shows the iris code for the frontal iris image, Fig. 12 (d) shows the iris code for the off-angle iris image, Fig. 12 (e) shows the frontal iris code generated by the Pix2Pix GAN



(a) (b) Fig. 13. (a) Performance of all subjects using ROC plots for off-angle images at +40° in angle. (b) Performance of all subjects using ROC plots for off-angle images at +50° in angle using Resized Iris code images.

367

368

369

370

371

372

373

374

375

376

377

378

379

380

model. Masks are applied in each iris image to discount the pixels covered by the eyelids. Fig. 12 (f) depicts the XOR result of Fig. 12 (c) and Fig. 12 (d), with the white pixels representing hits and red pixels representing misses. Fig. 12 (g) depicts the XOR result of Fig. 12 (c) and Fig. 12 (e) in a similar manner as above. The image in Fig. 12 (g) has more white pixels than the image in Fig. 12 (f). Also, there are a total of 41762 hits in the case of Fig. 12 (f), as opposed to a total of 46042 hits in the case of Fig. 12 (g), which shows the improved performance of the proposed model over the baseline, which compares the off-angle iris images with their frontal versions (40-degree). Unlike the previous model, this model exceeded baseline performance at positive gaze angles, as can be seen in Fig. 13. More specifically, the AUC increases from 0.999 to 0.9993 for +30° gaze angle images, from 0.9989 to 0.9995 for +40° gaze angle images, and from 0.9822 to 0.9898 for +50° gaze angle images. Similarly, the (Equal Error Rate) EER, which is the point where the FPR and False Negative Rate (FNR) are the same, also improves from 0.0075 to 0.0059 for +30° gaze angle images, from 0.0115 to 0.0055 for +40° gaze angle images, and from 0.0539 to 0.0432 for $+50^{\circ}$ gaze angle images. FNR can be defined as 1 - TPR. However, this method was only able to retain the performance at all the negative angles. For -30° and -50° gaze angle images, the AUC

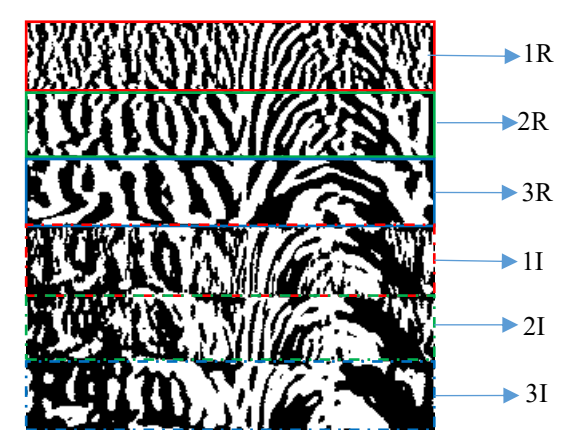


Fig. 14. An iris code with the different iris code strips description.

slightly decreased from 1 to 0.9997, and 0.9975 to 0.9972 respectively, but the model showcased improved AUC for -40° gaze angle images from 0.9998 to 0.9999. The results demonstrated that using iris codes for conversion would turn out to be a more reliable option than using normalized iris images for conversion.

4.3 Experiments for Conversion using Iris Code sub-blocks

Instead of resizing the iris codes to (256 x 256) images, this approach uses four of the six iris code strips. In this process, the normalized iris images obtained are sampled as (64 x 256) images, instead of (64 x 512) images. Using the six Gabor filters, six iris codes are then extracted. Using four of those six iris codes would result in (256 x 256) iris code images. Three of the six Gabor filters are labeled as real filters and the remaining three are labeled as imaginary filters. Each iris code strip obtained is labeled based on their order and the real/imaginary filter used to extract it, as shown in Fig. 14. The 1R, 2R, and 3R represent the three real iris code strips, and 1I, 2I, and 3I represent the three imaginary iris code strips.

To demonstrate the effect of this model, we use the test subject in Fig. 15 (a, b) and Fig. 16 (a, b).

Fig. 15 has the test subject at +50° gaze angle and Fig. 16 has the same test subject at +40° gaze

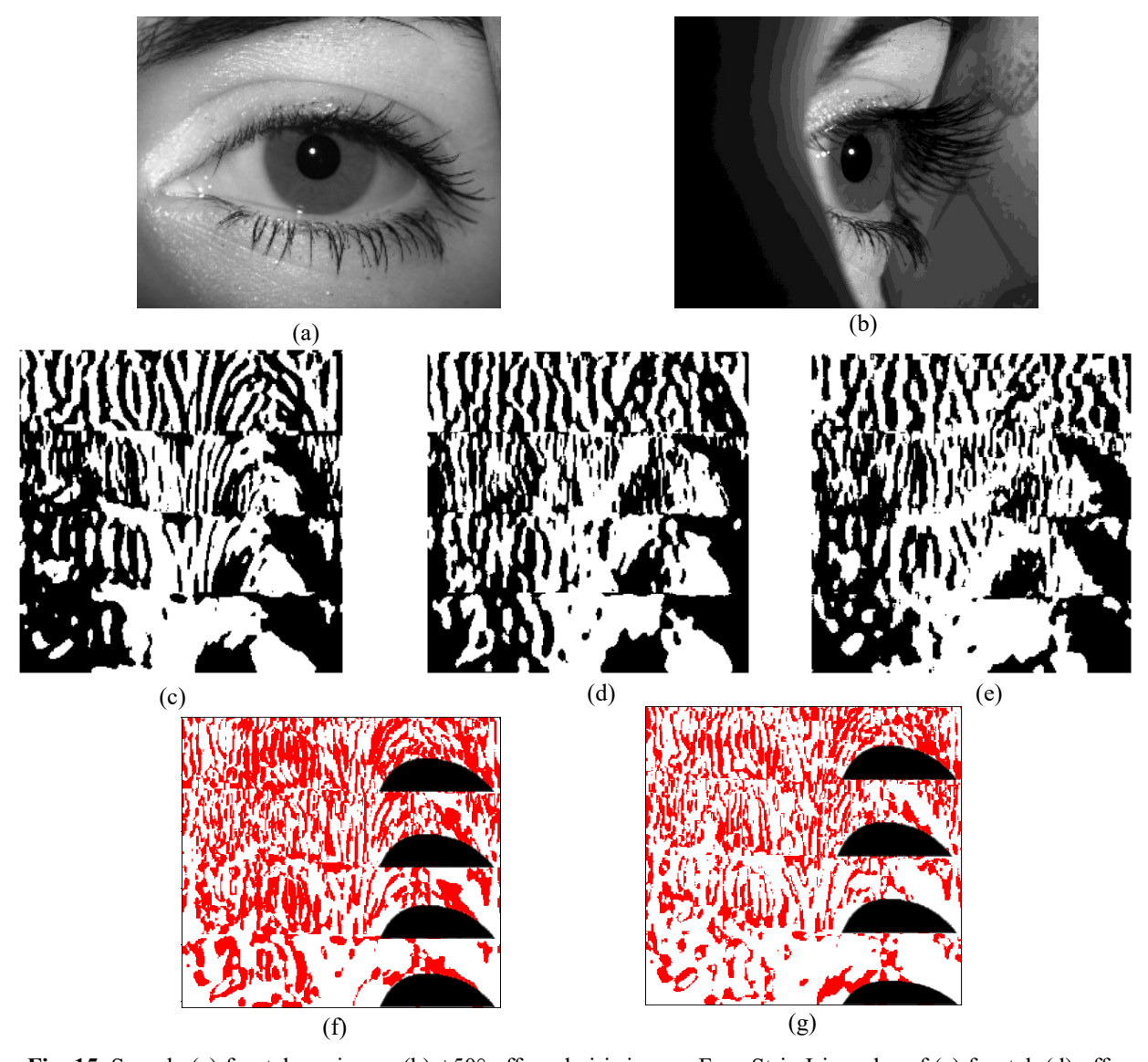


Fig. 15. Sample (a) frontal eye image (b) +50° off-angle iris image, Four Strip Iris codes of (c) frontal, (d) off-angle, (e) generated images. XOR comparison of (f) frontal and off-angle iris codes and (g) frontal and generated iris codes. Note that, red pixels are for different bits (misses), white for same bits (hits), and gray for the mask.

angle. Four iris strips corresponding to one real (1R) and three imaginary (1I, 2I, 3I) iris strips have been used for this part. Fig. 15 (c, d, e) and Fig. 16 (c, d, e) show the four-strip iris codes corresponding to the frontal image, off-angle image, and the generated frontal image. Fig. 15 (f) and Fig. 16 (f) shows the result of the comparison of frontal and off-angle iris images in Fig. 15 (c, d) and Fig. 16 (c, d), and Fig. 15 (g), Fig. 16 (g) show the result of the comparison of frontal

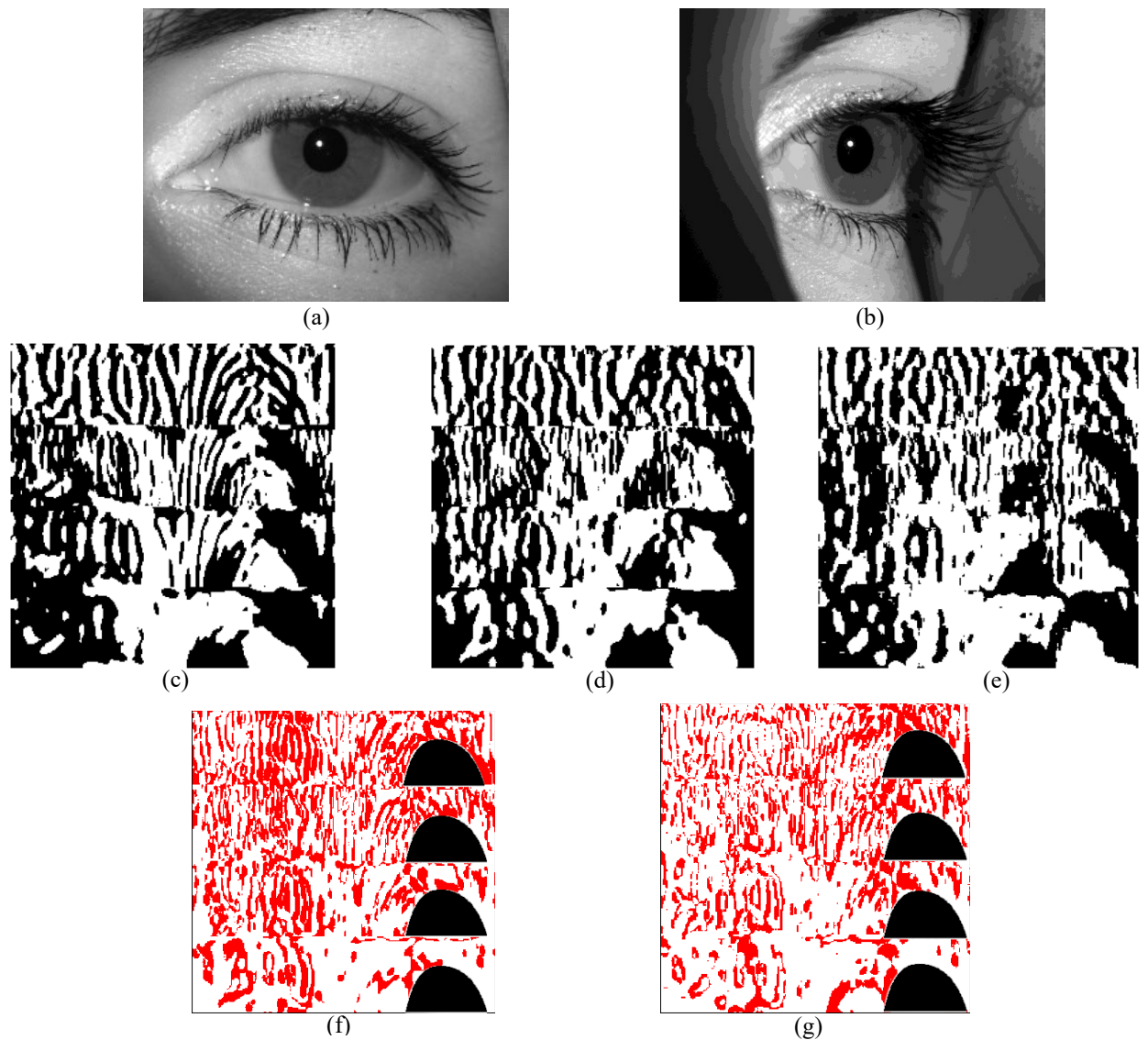


Fig. 16. Sample (a) frontal eye image (b) +40° off-angle iris image, Four Strip Iris codes of (c) frontal, (d) off-angle, (e) generated images. XOR comparison of (f) frontal and off-angle iris codes and (g) frontal and generated iris codes. Note that, red pixels are for different bits (misses), white for same bits (hits), and gray for the mask.

and generated frontal iris images in Fig. 15 (c, e) and Fig. 16 (c, e). The black portions in Fig. 15 (f, g) and Fig. 16 (f, g) are the masked portions due to the presence of eyelids. Even to the naked eye, Fig. 15 (g) and Fig. 16 (g) show better results than Fig. 15 (f) and Fig. 16 (f) as it has more of the whiter portion(hits) than the red portion(misses). Numerically, Fig. 15 (f) has 39667 hits, as opposed to 45249 hits for Fig. 15 (g), and Fig. 16 (f) has 41762 hits, as opposed to 46042 for Fig.

Table 1: Area Under Curve for different gaze angles and four strip iris codes. (Yellow highlights indicate the improvement compared to baseline, and the red text indicates sequences with at least four cases of improvements.)

	-30°	-40°	-50°	+30°	+40°	+50°
Sequence	AUC	AUC	AUC	AUC	AUC	AUC
1R2R1I2I	0.999969	0.999924	0.999557	0.999419	0.999839	0.994588
1R2R1I3I	0.999996	0.999976	<mark>0.999528</mark>	0.999655	0.999928	0.994138
1R2R2I3I	0.999955	0.999956	0.999266	0.999226	0.999809	0.992606
1R2R3R1I	0.999999	0.999998	0.999749	0.999849	0.999933	0.998619
1R2R3R2I	0.999990	0.999982	0.999728	0.999557	0.999941	0.997626
1R2R3R3I	0.999991	0.999992	0.999779	0.999566	0.999947	0.997361
1R3R1I2I	0.999972	0.999763	0.999503	0.999483	0.999941	0.996783
1R3R1I3I	0.999978	0.999956	0.999647	0.999803	0.999919	0.994523
1R3R2I3I	0.999834	0.999819	0.999219	0.999386	0.999714	0.997460
2R1I2I3I	0.999840	0.999584	0.998907	0.999391	0.999799	0.997250
2R3R1I2I	0.999983	0.999974	0.999761	0.999687	0.999968	0.997692
2R3R1I3I	0.999961	0.999862	0.999676	0.999603	0.813719	0.830316
2R3R2I3I	0.843166	0.887403	0.884059	0.908284	0.85933	0.902404
3R1I2I3I	0.794915	0.821343	0.818947	0.869981	0.815817	0.793587

16 (g). These numbers indicate that the generated iris images are much closer to the original frontal

iris image than the off-angle iris images. Picking four out of six iris codes would result in a total of $\binom{6}{4}$ combinations, which would result in 15 different models for each of the six angles (+50°,

+40°, +30°, -50°, -40°, and -30°).

Out of the total (15 x 6) = 110 combinations, a few combinations have exceeded the baseline performance. The baseline in this experiment refers to the iris recognition performance using the original (384 x 256) iris code strips, which have six iris code strips generated by the six Gabor filters.² The original off-angle performance for $+50^{\circ}$, $+40^{\circ}$, $+30^{\circ}$, -50° , -40° , and -30° is 0.995799, 0.999649, 0.999599, 0.999482, 0.999939 and 0.999981 respectively.

Their corresponding EERs are 0.026293, 0.004094, 0.003566, 0.009639, 0.002509, and 0.001455, respectively. When compared to these baseline values, several four-strip combinations as highlighted in yellow in Table 1 showed better performance. Most cases of improvement are found

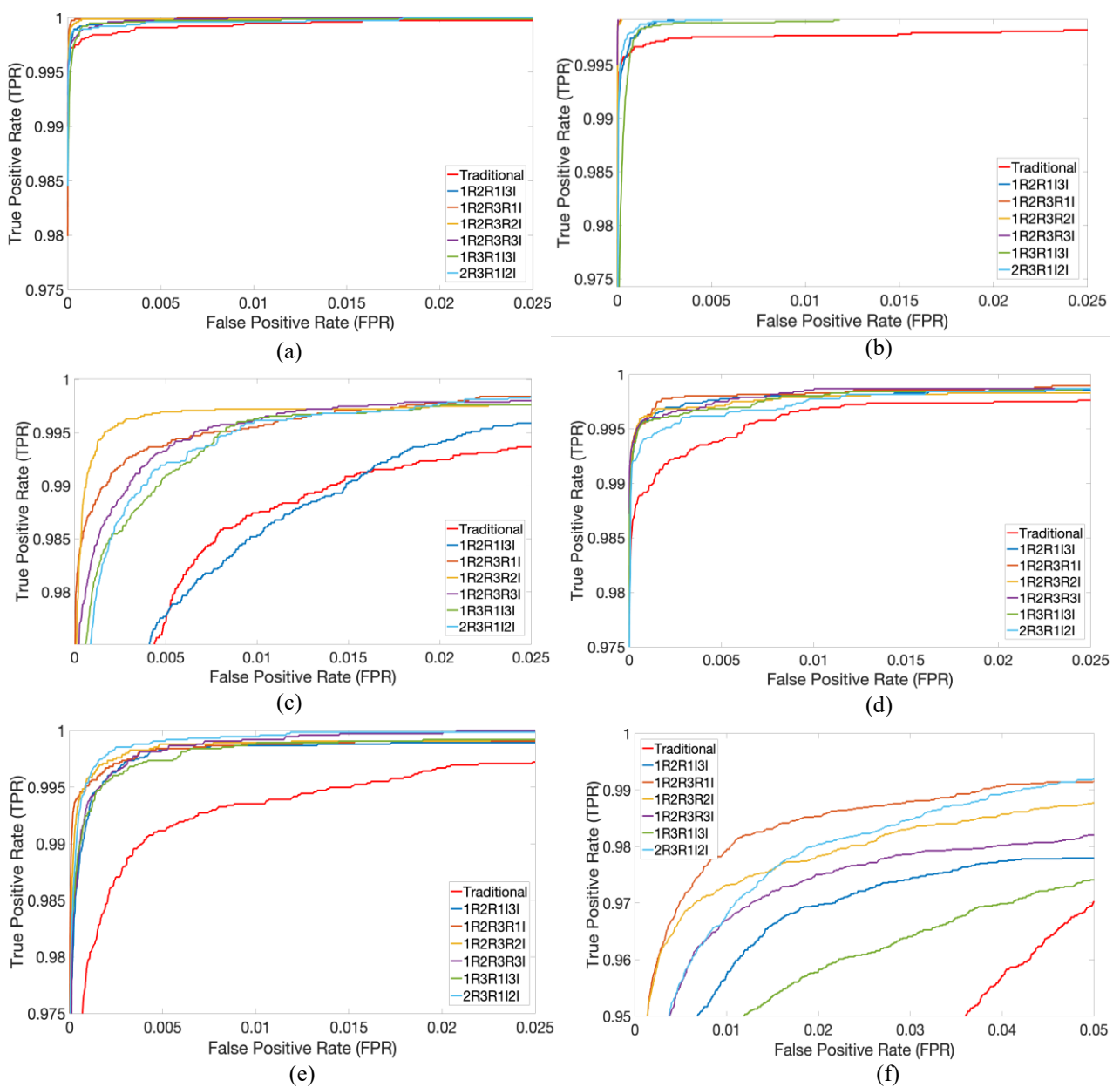


Fig. 17. Performance of all subjects for different 4-strip iris code combinations for angles: (a) -30° , (b) -40° , (c) -50° , (d) $+30^{\circ}$, (e) $+40^{\circ}$, (f) $+50^{\circ}$.

in the angle +40°, and the least cases of improvement are found in the angle -30°. The combinations highlighted in red have shown improvement in at least four out of the six gaze angles considered. The combination 1R2R3R1I, which is the set of the first four consecutive iris strips have shown improvement across all the gaze angles. When the three real iris strips are used in any combination,

they have shown an improvement in five out of the six gaze angles. Of the six iris strip combinations that are highlighted in red, four of them have at least three consecutive iris strips. This is an indication that using the real part of the iris code strips, and using three or more consecutive iris strips can lead to better overall improvement. Conversely, similar improvements are not observed with combinations involving the imaginary components of the iris strips.

Fig. 17 shows how the baseline performance varies with the gaze angle for each of the best six combinations from Table 1. For a -30° gaze angle, the original ROC curve is very close to the top left corner. Therefore, only four out of the six best combinations could show an improved ROC curve, more specifically, 1R2R1I3I, 1R2R3R1I, 1R2R3R2I, and 1R2R3R3I. The same is the case with +30°, where the combinations 1R2R1I3I, 1R2R3R1I, 1R2R3R1I, 1R2R1I3I, and 2R3R1I2I show improvement over the original. A clearer distinction can be found between the ROCs for the original and the generated iris codes for the extreme angles such as -40°, -50°, +40° and +50°. This shows that using this approach could pave the way for improved iris recognition at more extreme gaze angles.

5. Conclusion

This study aims to enhance off-angle iris recognition by projecting off-angle iris images to frontal iris images, improving the distinction between intra-class and inter-class Hamming distance scores for better recognition accuracy. Three different approaches utilizing a Pix2Pix GAN network with various loss functions were proposed. The first two approaches used resized normalized and resized iris code images. The model using resized normalized images showed improvements only with the extremely negative gaze angles, while the model using resized iris code images showed improvements only with the extremely positive gaze angles.

The third approach using subsampled four iris code images showed improvements across both the positive and the negative extreme gaze angles consistently. This approach can be further improved by selectively incorporating useful information from the skipped iris code portions. The drawback of utilizing four Iris Code strips instead of the six strips for iris recognition is the potential loss of valuable information. To address this and ensure the retention of information from all six strips of the iris code, a combination of two sub-blocks of iris code can be employed.

The first iris code strip can be denoted as the primary block, and the second iris code strip can be referred to as the secondary block. The primary block can be utilized in its entirety. The two missing strips from the primary block can be acquired from the secondary block and seamlessly integrated into their respective positions within the primary block. The resulting structure is a high-quality 6 * (64 x 256) iris code image that preserves all the iris information. Instead of choosing the secondary iris block at random for the two missing strips, a threshold-based system can be employed, where the resultant value of the best pixel at a point is based on the count of all the secondary pixels at that point. If the number of zero-value pixels of all the two-missing secondary iris strips for a point is greater than a threshold, the resultant value of the pixel at that point will be a zero. Similarly, if the number of one-value pixels of all the two-missing secondary iris strips for a point is greater than a threshold, the resultant value of the pixel at that point would be a one. However, if neither of the counts pass the threshold, the value of the resultant pixel would be a zero. An additional mask can be added to ensure that this conversion transitions smoothly.

While a separate CNN model was used to identify the gaze angle in this model for convenience, automating the process of gaze angle identification would significantly reduce the number of training models. Instead of a regular Pix2Pix GAN model, a Conditional Pix2Pix GAN model

468 which can take as input the gaze angle along with the pair of images would help make it a reality. 469 This can be done by concatenating the angle information along with the image features in the first 470 layer of the Pix2Pix GAN model. Now, the generator will take both the angle and off-angle image 471 as the input. The discriminator can also be trained to ensure that the generated images are realistic 472 for a given angle. Findings also highlight the significance of diverse loss functions capturing iris 473 textural characteristics and indicate that using real parts of iris code images makes for a better iris 474 recognition model. 475 Acknowledgments 476 This project was made possible by support from the SaTC program of NSF under grant awards 477 CNS-1909276 and CNS-2100483. 478 7. Data Availability 479 The iris images in the off-angle iris dataset will be available after publishing the paper on our lab's webpage.²⁵ 480 481 482 483 484 485

- 486 References
- 1. K. Nguyen et al., "Deep Learning for Iris Recognition: A Survey," Association for Computing
- 488 Machinery (ACM), 56(9), 1 35, https://doi.org/10.1145/3651306 (2024).
- 489 2. J. Daugman, "How Iris Recognition Works," IEEE Transactions on Circuits and Systems for Video
- 490 Technology, 14(1), 21-30, https://doi.org/10.1109/TCSVT.2003.818350 (2004).
- 3. C. Belcher and Y. Du, "Region-based SIFT approach to iris recognition," Optics and Lasers in
- 492 Engineering, 47(1), 139–147, https://doi.org/10.1016/j.optlaseng.2008.07.004 (2009).
- 493 4. A. Boyd et al., "Deep Learning-Based Feature Extraction in Iris Recognition: Use Existing Models,
- 494 Fine-tune or Train from Scratch?" in IEEE 10th International Conference on Biometrics Theory,
- 495 Applications and Systems (BTAS), 1-9, https://doi.org/10.1109/BTAS46853.2019.9185978 (2019).
- 496 5. Z. Luo et al., "A Deep Feature Fusion Network Based on Multiple Attention Mechanisms for Joint Iris-
- 497 Periocular Biometric Recognition," IEEE Signal Processing Letters, 28, 1060-1064,
- 498 https://doi.org/10.1109/LSP.2021.3079850 (2021).
- 499 6. J. Daugman, "New Methods in Iris Recognition," IEEE Transactions on Systems, Man, and
- 500 Cybernetics, Part B (Cybernetics), 37(5), 1167-1175, https://doi.org/10.1109/TSMCB.2007.903540
- 501 (2007).
- 7. J. Zuo et al., "A Robust IRIS Segmentation Procedure for Unconstrained Subject Presentation," in
- Biometrics Symposium: Special Session on Research at the Biometric Consortium Conference, 1-6,
- 504 https://doir.org/10.1109/BCC.2006.4341623 (2006).
- 8. X. Li et al., "A Feature-level Solution to Off-angle Iris Recognition," in International Conference on
- 506 Biometrics (ICB), 1-6, https://10.1109/ICB.2013.6612991 (2013).
- 9. H. J. Santos-Villalobos et al., "ORNL Biometric Eye Model for Iris Recognition" in IEEE Fifth
- International Conference on Biometrics: Theory, Applications and Systems (BTAS), 176-182,
- 509 https://doi.org/10.1109/BTAS.2012.6374574 (2012).

- 510 10. M. Karakaya et al., "Limbus impact on off-angle iris degradation," in International Conference on
- 511 Biometrics (ICB), 1-6, https://doi.org/10.1109/ICB.2013.6612971 (2013).
- 512 11. G. N. Cerme and M. Karakaya, "3D iris structure impact on iris recognition," in 23rd Signal
- Processing and Communications Applications Conference (SIU), https://doi.org/907-910,
- 514 10.1109/SIU.2015.7129977 (2015).
- 515 12. M. Karakaya, "Iris-ocular-periocular: toward more accurate biometrics for off-angle images," Journal
- of Electronic Imaging, 30, 033035 033035, https://doi.org/10.1117/1.JEI.30.3.033035 (2021).
- 13. E. Jalilian et al., "Deep Learning Based Off-Angle Iris Recognition," in IEEE International
- 518 Conference on Acoustics, Speech and Signal Processing (ICASSP), 4048-4052,
- 519 https://doi.org/10.1109/ICASSP43922.2022.9746090 (2022).
- 520 14. Z. Zhang et al., "Age Progression/Regression by Conditional Adversarial Autoencoder," in IEEE
- 521 Conference on Computer Vision and Pattern Recognition (CVPR), 4352-4360,
- 522 https://doi.org/10.1109/CVPR.2017.463 (2017).
- 523 15. F. Taherkhani et al., "Profile to Frontal Face Recognition in the Wild Using Coupled Conditional
- 524 GAN," IET Biometrics, 11(3), 260-276, https://doi.org/10.1049/bme2.12069 (2022).
- 525 16. P. Isola et al., "Image-to-Image Translation with Conditional Adversarial Networks," in IEEE
- 526 Conference on Computer Vision and Pattern Recognition, 5967-5976,
- 527 https://doi.ieeecomputersociety.org/10.1109/CVPR.2017.632 (2017).
- 528 17. J. S. Kota and M. Karakaya, "Challenges in Off-angle to Frontal Iris Image Conversion using Pix2Pix
- 529 Generative Adversarial Networks," in IEEE International Joint Conference on Biometrics (IJCB), 1–8,
- 530 https://doi.org/10.1109/IJCB57857.2023.10448976 (2023).
- 18. K. Diab and M. Karakaya, "CNN-Based Gaze Estimation for Off-angle Iris Recognition," IEEE
- 532 SoutheastCon, 736-742, https://doi.org/10.1109/SoutheastCon48659.2022.9763926 (2022).

- 533 19. E. Ehrlich and M. Karakaya, "Comparison of elliptical unwrapping and frontal projection for off-
- angle iris normalization," Disruptive Technologies in Information Sciences V, 11751,
- 535 https://doi.org/10.1117/12.2588898 (2021).
- 536 20. Z. Wang et al., "Image Quality Assessment: From Error Visibility to Structural Similarity," in IEEE
- 537 Transactions on Image Processing, 13(4), 600-612, https://doi.org/10.1109/TIP.2003.819861 (2004).
- 538 21. M. Karakaya, "A study of how gaze angle affects the performance of iris recognition," Pattern
- 539 Recognition Letters, 82(2), 132–143, https://doi.org/10.1016/j.patrec.2015.11.001 (2016).
- 540 22. M. Arjovsky et al., "Wasserstein Generative Adversarial Networks," Proceedings of the 34th
- International Conference on Machine Learning, 70, 214-223,
- 542 https://doi.org/10.48550/arXiv.1701.07875 (2017).
- 23. M. M. Tai, "A Mathematical Model for the Determination of Total Area Under Glucose Tolerance
- and Other Metabolic Curves," 152–154 (1994) [doi:10.2337/diacare.17.2.152].
- 545 24. M. Moshirfar, R. N. Hoggan, and V. Muthappan, "Angle Kappa and its importance in refractive
- 546 surgery," 151–158, India (2013) [doi:10.4103/0974-620X.122268].
- 547 25. https://facultyweb.kennesaw.edu/mkarakay/iris.php

550

551

552

553

554

555

556

557

558 List of Figures

- Fig. 1. General process of iris recognition.
- Fig. 2. Different domains for iris image conversion (a) Captured original image (b) Ocular iris
- image (c) Normalized iris image (d) Iris code with six channels.
- Fig. 3. Approaches to frontal iris conversion using Normalized iris images (blue) and using Iris
- 563 Code images (orange).
- Fig. 4. A test subject's (a) Off-angle iris image (b) Original iris code (384 x 512) (c) Resized iris
- 565 code (256 x 256).
- Fig. 5. Choosing sub-blocks of iris code: (a) Original iris code with six channels (384 X 256) (b)
- Iris code sub-block with 4 channels (256 X 256).
- Fig. 6. (a) Experimental setup of off-angle image capturing (b) Illustration of the movement of the
- 569 camera
- 570 Fig. 7. Baseline ROC curves for all the subjects in (a) Negative gaze angles (b) Positive gaze
- 571 angles
- Fig. 8. A test subject's (-40° gaze angle) (a) Frontal iris image (b) Off-angle iris images (c, h)
- Resized frontal normalized iris images (d) Resized off-angle normalized iris image (e, j) Generated
- 574 normalized iris image.
- Fig. 9. Distributions of hamming distance scores for: (a) the frontal vs. off-angle iris images (-50°
- in angle) (b) the frontal vs. generated frontal images for the test subject (c) Performance analysis
- using ROC plots images at -50° in angle vs. generated frontal images for the test subjects.
- Fig. 10. Performance analysis using ROC plots for off-angle images at -50° in angle for different
- 579 loss functions.
- Fig. 11. Performance analysis of all subjects using ROC plots for off-angle images at (a) -40° (b)
- -50° (c) $+40^{\circ}$ (d) $+50^{\circ}$ in angle using Resized Normalized iris images.
- Fig. 12. A test subject's: (a) Frontal eye image (b) Off-angle iris image, Iris codes of (c) frontal,
- (d) off-angle, (e) generated images. XOR comparison of (f) frontal and off-angle iris codes and (g)
- frontal and generated iris codes. Note that, red pixels are for different bits (misses), white for same
- 585 bits (hits), and gray for the mask.
- 586 Fig. 13. (a) Baseline Performance analysis using ROC plots for off-angle images at different
- positive in angles. (b) Performance of all subjects using ROC plots for off-angle images at +40°
- in angle. (c) Performance of all subjects using ROC plots for off-angle images at +50° in angle
- using Resized Iris code images.
- 590 **Fig. 14.** An iris code with the different iris code strips description.
- Fig. 15. A test subjects' (+50° gaze angle) (a) Frontal eye image (b) Off-angle iris image, Four
- 592 Strip Iris codes of (c) frontal, (d) off-angle, (e) generated images. XOR comparison of (f) frontal

593 and off-angle iris codes and (g) frontal and generated iris codes. Note that, red pixels are for different bits (misses), white for same bits (hits), and gray for the mask. 594 Fig. 16. A test subjects' (+40° gaze angle) (a) Frontal eye image (b) Off-angle iris image, Four 595 596 Strip Iris codes of (c) frontal, (d) off-angle, (e) generated images. XOR comparison of (f) frontal 597 and off-angle iris codes and (g) frontal and generated iris codes. Note that, red pixels are for different bits (misses), white for same bits (hits), and gray for the mask. 598 599 Fig. 17. Performance of all subjects for different 4-strip iris code combinations for angles: (a) -600 30° , (b) -40° , (c) -50° , (d) $+30^{\circ}$, (e) $+40^{\circ}$, (f) $+50^{\circ}$. 601 602 Table 1 Area Under Curve for different gaze angles and four strip iris codes. (Yellow 603 604 highlighted cells indicate improvement over baseline, and the red text indicates sequences with at least four cases of improvement over the baseline) 605 606